Biocompatibility of nitrogen-doped multiwalled carbon nanotubes with murine fibroblasts and human hematopoietic stem cells

Jose G. Munguia-Lopez[1,2], Rodrigo Juarez[1], Emilio Muñoz-Sandoval[3], Marco A. Kalixto Sanchez[4], Joseph Matthew Kinsella[2], Antonio De Leon-Rodriguez[1]*

[1]Department of Molecular Biology, Instituto Potosino de Investigación Científica y Tecnológica, A.C. Camino a la Presa San José 2055, Lomas 4 sección, 78216, San Luis Potosí, Mexico; jose.munguia-lopez@mcgill.ca; jmunguialopez@gmail.com

[2]Department of Bioengineering, McGill University, 817 Sherbrook Street West, Montreal, Quebec, H3A 0C3, Canada.

[3]Advanced Materials Department, Instituto Potosino de Investigación Científica y Tecnológica, A.C. Camino a la Presa San José 2055, Lomas 4 sección, 78216, San Luis Potosí, Mexico.

[4]Hospital General del ISSSTE, Carlos Diez Gutiérrez 915, Col. Julian Carrillo CP 78340, San Luis Potosi, México.

***Correspondence: aleonr@ipicyt.edu.mx; aleonr@me.com; Tel:+52 444 834 2058. Fax:+52 444 834 2010

JGML: orcid.org/0000-0002-5173-6494
RJ: orcid.org/0000-0003-4324-3902
EMS: orcid.org/0000-0002-6095-4119
JMK: orcid.org/0000-0002-3052-0782
ALR: orcid.org/0000-0003-3347-3499

Abstract Carbon nanotubes (CNTs) are one of the most attractive nanomaterials for both industrial and biomedical applications because of their physicochemical properties. These nanomaterials can be synthesized by chemical vapor deposition (CVD) in small and large production (laboratory and industry, respectively). However, this synthesis method generates heterogeneous nanomaterials that could lead to different cellular responses giving inconsistencies and even contradictory results. In this work, the biocompatibility of nitrogen-doped multiwalled carbon nanotubes (CN_x) with murine fibroblasts and human hematopoietic stem cells (hHSC) was evaluated. CN_x were synthesized by CVD method; then, purified, characterized, and classified in three fractions designed as Small CN_x (S-CN_x), Medium (M-CN_x) and Large (L-CN_x). Mammalian cells were incubated with CN_x in the range of 0.07 to 70 µg/mL, and cell viability was evaluated. M-CN_x were biocompatible with both murine fibroblasts and hHSC, whereas, S-CN_x and L- CN_x showed a cytotoxic effect. In this work, it has been demonstrated that CNTs produced by CVD have differences on the biocompatibility with mammalian cells, but the M-CN_x could be a great candidate for biomedical applications.

Keywords Nanomaterial, nitrogen-doped carbon nanotubes, murine cells, stem cells.

Acknowledgments The authors thank The Marcos Moshinsky Foundation, CONACYT-Mexico CB-2013-220744 for partial funding and CONACYT for the scholarship 250279. Also, the authors thank L. Aldana and Abdullah Chaudhary for the English review and V. Balderas for his technical assistance.

Introduction

Carbon nanotubes (CNTs) are cylindrical hollow graphene sheets of one or more layers denoted as single-wall (SWCNTs) or multiwall (MWCNTs). Both SWCNTs and MWCNTs have lengths ranging between hundreds of nanometers to centimeters with diameters oscillating from 0.4-2 nm and 2-200 nm for SWCNTs and MWCNTs, respectively (Cui et al. 2010). CNTs are a novel promising material for bioimaging, biosensing, scaffold, and biomedical applications, due to their mechanical, electrical and optical properties (De Volder et al. 2013; Ferreira et al. 2008; Mundra et al. 2014). Since the similarity of CNTs and their shape with the asbestos fibers, which represent a risk for human health, CNTs must be tightly tested before using them for *in vivo* applications (Fisher et al. 2012; Mihalchik et al. 2015). Biocompatibility of CNTs has been related to their dimension (Mihalchik et al. 2015; Sohaebuddin et al. 2010), synthesize method, functional groups (Carrero-Sanchez et al. 2006; Zhao and Liu 2012), agglomeration degree(Kunzmann et al. 2011; Sabuncu et al. 2010), concentration, and time of exposure (Lanone et al. 2013; Liu et al. 2013; Sohaebuddin et al. 2010).

To make CNTs biocompatible with the mammalian cells(Li and Niu 2003; Zhao et al. 2011b) or whole organisms (Carrero-Sanchez et al. 2006), different strategies have been successfully employed using chemical surface modification by addition of functional groups such as carboxyl or hydroxyl to the sidewall of CNTs (He et al. 2017; Liu et al. 2014; Liu et al. 2016b) and Mussel-inspired chemistry, allowing better dispersion and biocompatibility of nanomaterials (Huang et al. 2018; Liu et al. 2015; Liu et al. 2016a; Zhang et al. 2017; Zhang et al. 2012c). Doping is another chemical strategy for introducing heteroatoms into the CNT structure. Chemical vapor deposition (CVD) is one of the most common methods to synthesize nitrogen-doped CNTs (CN_x) at large scale (Bazargan and McKay 2012; Mubarak et al. 2014; Nxumalo et al. 2008; Shah and Tali 2016). However, the synthesis of CNTs by CVD produces a variety of morphologies with different diameters and lengths as well as different types of CNTs in the same batch when the carbon precursor or catalyst source changes (Meysami et al. 2013b; Munguía-Lopez et al. 2015). This heterogeneity could produce various cellular responses.

Here, the synthesis of CN_x by CVD and their physicochemical characterization are reported, as well as their biocompatibility with murine fibroblasts and human hematopoietic stem cells (hHSC) (Fig. 1). Murine fibroblast cells were chosen as biological model since they can be found in the majority of tissues and organs of the body associated with extracellular matrix molecules (Krenning et al. 2010; McAnulty 2007) and they can be a good model for cell adhesion studies. For cellular uptake experiments, murine macrophages were selected due to their ability to phagocyte and stimulate body response against foreign materials (Canapè et al. 2015). Another attractive cell model for biocompatibility assays is hHSC. These cells are self-renewing, tissue-specific stem cells that lay the foundation of hematopoiesis to generate all functional mature blood cell types (Kim et al. 2014; Wai Feng Lim et al. 2013). hHSC can be obtained from different sources such as bone marrow, mobilized peripherical blood and umbilical cord blood, and has been used as an invaluable treatment for malignant and non-malignant blood disorders due to their regenerative capacity to reconstitute the entire adult hematopoietic system after transplantation (Andrade-Zaldívar et al. 2011; Bari et al. 2013; Kim et al. 2014).

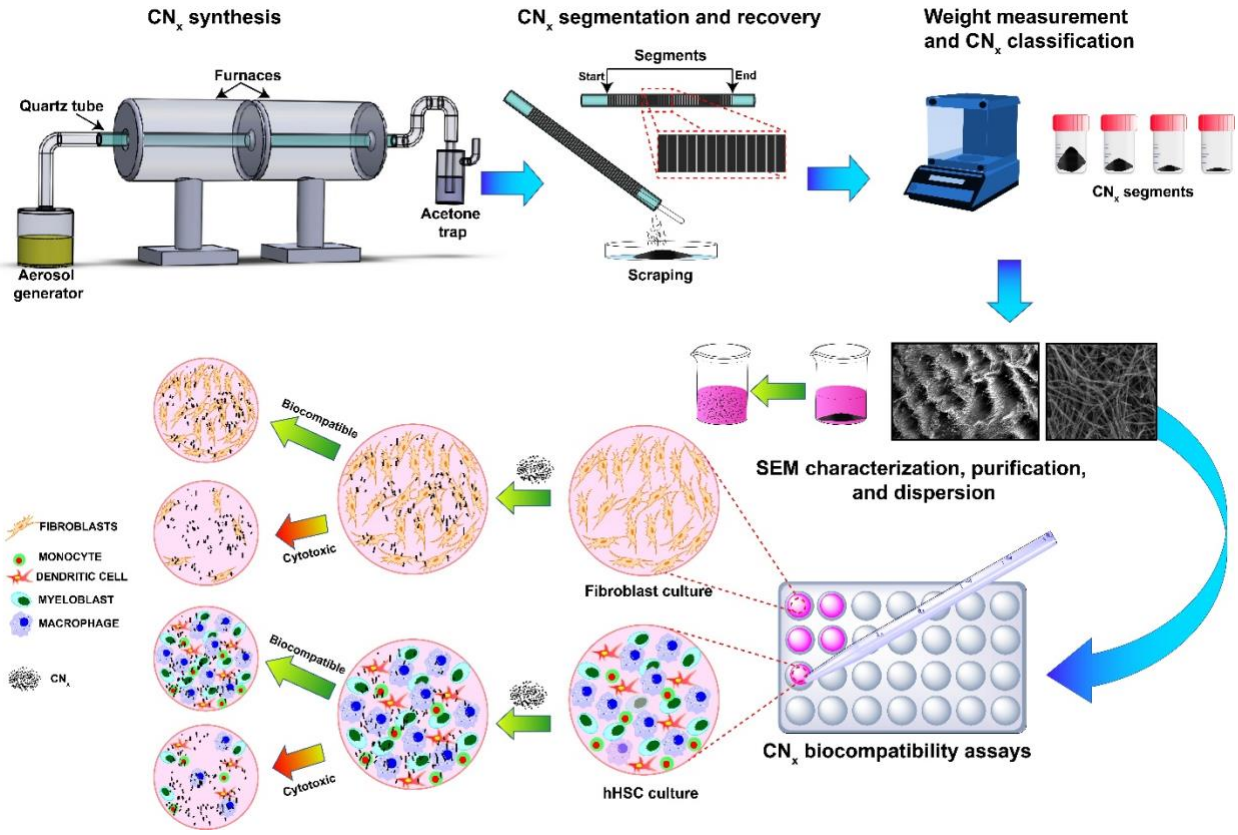

Fig. 1 Schematic illustration of CN_x synthesis, segmentation, physicochemical characterization, and biological assays performed to determine the biocompatibility of CN_x segments

In this work, it is shown that CVD method produces CN_x with different sizes and morphologies in the same batch. These CN_x promote different cellular response showing both biocompatibility and cytotoxicity on fibroblast. However, one of the CN_x segments shows biocompatibility, high-affinity for cell attachment, and cellular uptake, suggesting that this segment could be a great candidate for biomedical applications in a short future.

Materials and methods

Synthesis and purification of CN_x

Chemicals were purchased from Sigma-Aldrich in analytical grade. CN_x were synthesized by using the CVD method as described previously (Kamalakaran et al. 2000). The CVD system consisted of an aerosol generator and a 100-cm-long quartz tube placed inside of two 80-cm-long horizontal tube furnaces together. Prior to CN_x synthesis, the two furnaces were heated to 850°C keeping the temperature constant. The chemical precursors used were 2.5 % ferrocene in benzylamine, and the mix was placed into the piezo-driven aerosol generator. The spray was generated by argon at 2.5 L/min through the quartz tube. After 30 min of synthesis, the quartz tube was cooled down at room

temperature (RT) and washed with ethanol to remove residual liquids. Also, acetone was used to eliminate carbonaceous material and non-add CN_x.

For CN_x recovery, the quartz tube was divided into segments of 1 cm each one; then, each segment was scraped to collect the CN_x separately. Samples were weighed to obtain the yield of CN_x synthesis. Total product was classified based on their weight in three fractions designed as Small CN_x (S-CN_x), Medium CN_x (M-CN_x) and Large CN_x (L-CN_x), respectively (See results and discussion section). One segment from each fraction was characterized and used in biocompatibility experiments. CN_x fractions were sonicated by ultrasonic bath operating at 100 W and 42 kHz (Branson 2510 Ultrasonic Cleaner) in the presence of absolute ethanol during 1 h at RT and filtrated using 0.45 µm membrane filters. Then, the CN_x were recovered from membranes and put into an Erlenmeyer flask where they were purified by acid treatment of HNO_3:H_2SO_4 (1:3) using sonication for 12 h on ice. Purified CN_x were diluted with distilled water, kept on repose during 48 h and filtered through 0.45 µm membrane filters. Supernatant and sediment were treated as separate samples. For the biological assay, sediment samples were chosen.

Material characterization

CN_x were characterized by scan electron microscopy (SEM) to determine lengths, diameters, and energy-dispersive X-ray (EDX) spectrum (SEM, Philips-XL 30 SFEG; Dual Beam (FIB/SEM) FEI-Helios Nanolab 600 equipped with an EDX detector). To investigate their chemical composition, Fourier transformant infrared spectroscopy (FTIR) was performed on purified CN_x powder using an FTIR-ATR spectrophotometer (Nicolet 6700/Smart iTR, Thermo Scientific); the absorbance results were plotted within a wavelength range of 4000 to 600 cm^{-1}.

Dispersion of CN_x fractions in culture medium

CN_x fractions were dispersed separately in basal Iscove's Modified Dulbecco's Medium (IMDM) pH 7.2 supplemented with 10% fetal bovine serum (GIBCO), 100 U/mL penicillin, 100 µg/mL streptomycin and 0.25 µg/mL amphotericin B at a final concentration of 1 mg/mL. Samples were sonicated by an ultrasonic bath at 40°C during 8 h, resulting in a stable dispersion with no visible macro-agglomerates of CN_x. Then, the stocks were storage at 4°C until used.

Cell cultures

NIH-3T3 murine fibroblasts (ATCC) were defrosted and cultured in basal-IMDM into 24-well plates (Corning) over a period of 72 h in a humidity chamber at 37°C and CO_2 5% (Shell-Lab). After three passes, when 80% of cellular confluence was reached, cells were harvested with trypsin-EDTA.

To obtain the human hematopoietic stem cells (hHSCs) from umbilical cordon blood (UCB) samples from full-term deliveries were kindly provided by the ISSSTE regional hospital, according to their ethical committee's

guidelines. Separation of mononuclear cells (MNC) from UCB was carried using the procedure previously (Andrade-Zaldívar et al. 2011). Briefly, 20-45 mL blood samples with heparin (2,000 UI) were centrifuged at 450 *g* for 15 min, and the 4-6 mL of with interphase cells and plasma were transferred into a 15-mL falcon tube containing the same volume of phosphate-buffered saline (pH 7.2). Samples were mixed gently and transferred into 15-mL falcon tubes with 7 mL of Ficoll-Paque Plus (Pharmacia) at temperature room and centrifuged for 20 min at 550 *g*. MNC ring was recovered, put into clean tubes and centrifuged at 800 *g* for 15 min. MNC were resuspended in 1 mL of basal-IMDM supplemented with human recombinant cytokines: (Peprotech) 5 ng/mL stem cell factor (SCF), 5 ng/mL flt3 ligand (Flt-3), 5 ng/mL interleukin-3 (IL-3), 12.5 ng/mL interleukin-6 (IL-6), 10 ng/mL granulocyte-macrophage colony stimulation factor (GM-CSF),10 ng/mL granulocyte-colony stimulation factor (G-CSF), 3 U/mL erythropoietin (EPO, Bioyetin®).

Evaluation of biocompatibility of CN_x with NIH-3T3 murine fibroblasts and hHSCs

To evaluate the effect of the CN_x fractions, NIH-3T3 fibroblast cells with a density of $2x10^3$ cells per well were added to 96 well plates and pre-incubated 24 h at 37°C and 5% CO_2 atmosphere. Then, CN_x at a final concentration between 0.07-70 µg/mL were added into cultures and incubated again for 96 h. Samples were taken each 24 h, and cell viability was determined by cell counting with the trypan blue exclusion method using a hemocytometer. NIH-3T3 cell cultures without nanomaterial were used as a control. Exposure route experiments were carried out following Munguía-Lopez et al. (2015) methodology. Confluent fibroblasts were trypsinized and transferred to new 96-well plate $2x10^3$ cells per well; then, immediately after cell liftoff, CN_x were added to wells using the same concentration above mentioned. To avoid the variation on CN_x concentration in cell cultures when the medium is changed, kinetics carried out at work volume of 250 µL without medium replacement.

For hHSCs experiments, $0.5x10^6$ cells/mL were seeded onto 24 well plates and incubated for cellular recovery process (4-5 days at 37°C and 5% CO_2). After, the medium was changed with fresh basal-IMDM supplemented with cytokines and cells were counted again. Cells were exposed to M-CN_x fraction at final log concentration of 0.07-70 µg/mL during 120 h. Samples were taken each 24 h, and cell viability was determined by cell counting with the Trypan blue exclusion method using a hemocytometer. Cell cultures without nanomaterial were used as control. To avoid variation on CN_x concentration in cell cultures when the medium is changed, kinetics carried out at work volume of 1,100 µL without medium replacement. At the end of the kinetic, tumor necrosis factor alpha (TNF-α) was measured using human TNF-α ELISA development kit (Peprotech) in cultures containing CN_x 70 µg/mL and control. Light microscopy was used to analyze cell morphology and CN_x uptake after incubation.

CN_x cellular uptake and extraction of CN_x embedded by hHSCs

Murine macrophages J774a.1 cell line was used as a biological model for cellular uptake experiments. Macrophages were cultured in basal-IMDM at 50,000 cell/well in a 6-well plate during 24 h at 37°C and 5% CO_2; S-CN_x, M-CN_x or L-CN_x were added to cultures at a final concentration of 70 µg/mL and incubated for 24 h and 48 h.

After incubation, cells were washed three times with PBS to remove any residual CN_x not internalized by cells. The cells were then harvested by adding trypsin-EDTA solution, centrifuged at 840 g for 10 min, and the supernatant was discarded. For cell lysis, the pellet was resuspended in PBS and sonicated by ultrasonic bath operating at 100 w during 20 min on ice. The cell lysate was centrifuged at 7,500 g for 30 min, and CN_x were washed three times with PBS and resuspended in 200 µl of basal-IMDM. To quantify the CN_x uptaken by cells, Ultraviolet-Visible-Near Infrared (UV-Vis-NIR) spectroscopy was performed in the range of 600-800 nm (UV-Visible-NIR spectrometer, Lambda 750, Perkin Elmer), since cellular components (such as proteins and water) have almost no absorption in the NIR region (Weissleder 2001), and CN_x have very high absorbance (Ryabenko et al. 2004; Zhang et al. 2018). The concentration of CN_x per cell was estimated based on the corresponding calibration curve generated at the absorbance of 750 nm; the concentration was calculated as follows (Zhang et al. 2018):

$$cellular\ uptake\ \left(\frac{g}{cell}\right) = \frac{concentration\ of\ CNx\left(\frac{g}{L}\right) \times Volume\ (L)}{number\ of\ cells}$$

After hHSCs culture, cells were washed gently three times with PBS. All the adherent cells containing CN_x were incubated with trypsin for 10 min and recovered by pipetting, transferring the total volume into Eppendorf tubes. Samples were centrifuged at 840 g for 10 min. The supernatant was discarded, and the cells were rewashed with PBS extensively, and cells were resuspended in PBS and sonicated by ultrasonic bath. After sonication, the samples were centrifuged at 7,500 g for 30 min, and CN_x were washed with distilled water three times. CN_x samples were loaded into pins and visualized by SEM.

Statistics

Data are presented as mean ± standard deviation. Statistical comparison was performed with the 2-ways ANOVA. Dunnett and Bonferroni post-tests were used to compare treatment groups to control where $(*)$ asterisk indicates a significant difference (P-values < 0.05).

Results and discussion

Production and size determination of CN_x

CN_x segments from different batches were weighed individually and plotted to obtain a pattern of production. Fig. 2 shows a plot of CN_x segment weight and the morphology of the nanotubes for a typical batch. Three batches were synthesized, and the total amount produced was 789.26±99.09 mg/batch, where the yield of CN_x in the furnace 1 was 694.5±78.5 mg and 94.8±22.7 mg for the furnace 2, showing Gaussian distribution and maximum production of nanomaterials in the first 40 segments (Fig. 2a). According to this, the synthesis procedure used in this work was reproducible in terms of production (Meysami et al. 2013b). Based on the CN_x weight, the nanomaterials were classified into three fractions: 1) Small CN_x(S-CN_x), that corresponded to the segments 6-10 and 29-76, and recovered amount was 15 or less mg/segment ; 2) Large CN_x (L-CN_x) including segments 11-13 and 24-28 (15 to 30

mg/segment) and 3) Medium CN_x (M-CN_x) for the segments 14-23, and the amount recovered was >30 mg/segment (Fig. 2a). Each fraction was homogenized and characterized as described in the materials and methods section.

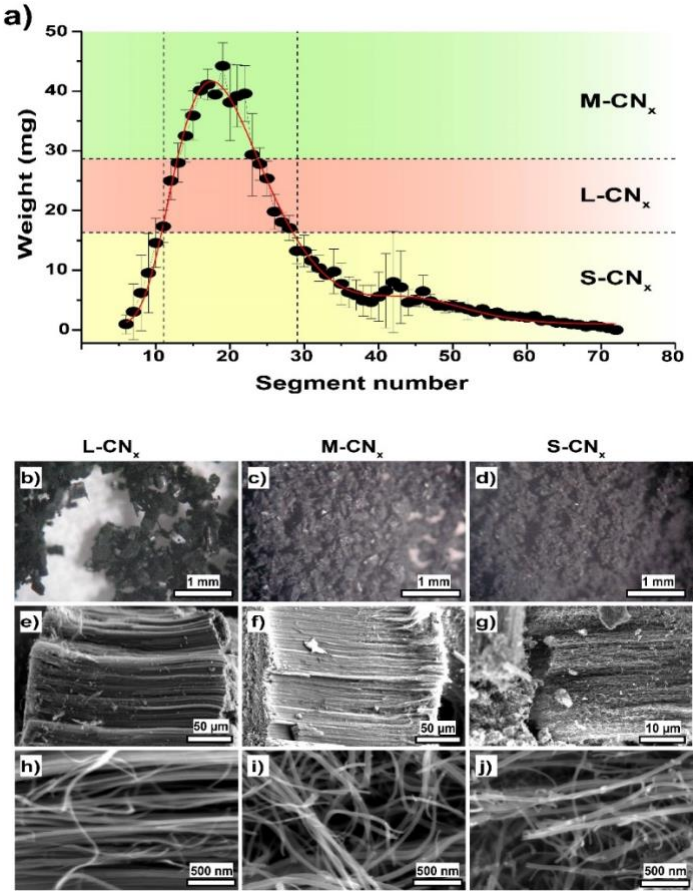

Fig. 2 a Production and weight of CN_x segments collected from three batches. Dotted lines display the segment classification with similar sizes and weight; color background indicates their biocompatibility. **b-d** optical and **e-j** SEM images of the morphology of L-CN_x, M-CN_x and S-CN_x from batch I

CNTs have exceptional physicochemical properties that make them attractive for biomedical application. CVD is one of the most common methods employed for CNTs synthesis (Jourdain and Bichara 2013), but this methodology can generate nanomaterial with different sizes and morphologies (Meysami et al. 2013a). Also, it has been reported that CNTs total mass production is altered by the carbon source used, where a total yield of the nanomaterials can be ranging from 57 to 1,000 mg (Meysami et al. 2013b). In terms of CN_x mass production, our synthesis procedure was reproducible, producing more than 800 mg/batch. During the size and morphological characterization of CN_x, we found nanotubes with different morphologies and sizes depending on the site of synthesis.

Optical and SEM images of the three fractions from batch I are shown in Fig. 2b-d and Fig. 2e-j. The lengths of CN_x from S-CN_x, M-CN_x, and L-CN_x fractions were 33.52 ± 0.92, 169.20 ± 9.68, and 236.53 ± 6.62 µm, respectively, with diameters of 50.04 ± 5.83, 52.67 ± 9.36 and 28.05 ± 4.36 nm for S-CN_x, M-CN_x and L-CN_x fractions. This nanomaterial heterogeneity could lead different effects on cellular response. Similar to these results, Meysami et al. (2013a) reported that synthesis of CNTs by CVD produces different morphologies and diameters of

CNTs. The authors found the diameter of the CNTs decrease as a function of distance from the beginning of the reactor, and CNTs deposited at 10 cm, and 60 cm of the reactor present significantly different *D/G* ratios.

The chemical composition of L-CN_x, M-CN_x, and S-CN_x was analyzed by FTIR (Fig. 3). The bands at ≈3700 cm^{-1} are assigned to the stretching of the bonding -OH groups (Escobar Barrios et al. 2012; Tucureanu et al. 2016). Between 3350-3310 cm^{-1}, the band of N-H stretch appears corresponding to secondary amine; this band is absent in S-CN_x sample. At ≈2800 cm^{-1} the C-H stretch peaks were detected in the three samples(Wu et al. 2006). The peaks at 2400-2000 cm^{-1} correspond to the characteristic C≡N stretching vibration (Escobar Barrios et al. 2012; Liao and Pan 2011), while C=N stretching mode appeared at ≈1650 cm^{-1}. The signal around ≈1800 cm^{-1} is assigned to C=O stretch and the band around ≈1500 cm^{-1} is attributed to NO_2 generated by acid purification/oxidation process (Escobar Barrios et al. 2012). The peak at ≈1350 cm^{-1} can be assigned to N-CH_3 (Tucureanu et al. 2016) or sulfate groups, a product of acid purification/oxidation treatment (Jiang et al. 2003). Finally the bands between 1100-900 cm^{-1} correspond to the N heterocyclic ring modes (Liao and Pan 2011). Comparing the absorption intensity of the peaks in the range of 2400-2000 cm^{-1}, the M-CN_x presented more C≡N bonds than L-CN_x, and L-CN_x showed more C≡N bonds than S-CN_x.

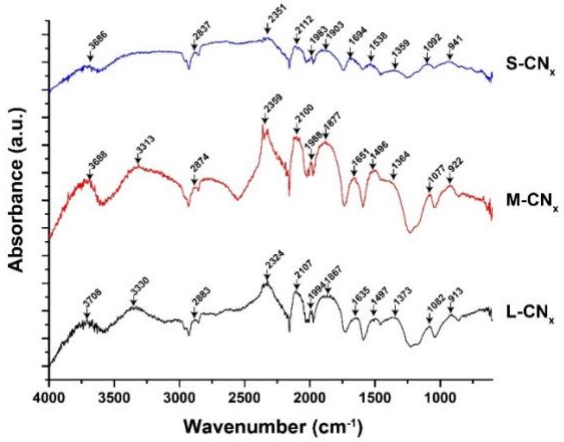

Fig. 3 FTIR spectra of the purified S-CN_x, M-CN_x, and L-CN_x

Effect of CN_x on NIH-3T3 murine fibroblasts

Different strategies have been developed to increase the biocompatibility of nanomaterials such as surface chemical modification by addition of polymers (Canapè et al. 2015; Shi et al. 2017), tannic acid (Zhang et al. 2015), functionalization (He et al. 2017; Liu et al. 2014; Liu et al. 2016b; Zhang et al. 2011b) with different functional groups or dispersion in culture medium containing serum proteins (Zhang et al. 2011b; Zhu et al. 2009). In this study, the CN_x were dispersed in culture medium supplemented with fetal bovine serum to allow well dispersion of the nanomaterials. Fig. 4 shows the growth cell kinetics of NIH-3T3 fibroblasts exposed to CN_x from batch I. After 96 h, control cultures reached 1.24±0.15 x10^5 cells/well. Cells incubated with S-CN_x grew less than control, and statistical differences were observed at 72 and 96 h of culture (Fig. 4a). S-CN_x used in the range of 0.07 to 7 μg/mL, inhibited partially the cell growth and a maximum cell density of 0.89±0.12 x10^5 cells/well was reached at the lower

S-CN_x concentration, whereas 70 µg/mL affected dramatically the cell growth and only 0.15±0.02 x10^5 cells/well were achieved after 96 h of culture. As noted in Fig. 4b no effect in the range of 0.07 to 70 µg/mL of M-CN_x on the cell growth was observed and the cultures grew reaching a maximum cell density of 1.14±0.1 x10^5 cells/well, similar to the control cultures (0.97±0.15 x10^5 cells/well). Contrary to this, L-CN_x affected slightly the cell growth, and statistic differences were observed at all exposure times and CN_x concentrations evaluated (Fig. 4c). However, these negative effects were lower than the effect obtained with S-CN_x at 70 mg/mL. These results indicate the biocompatibility of CN_x depends on the size of the nanomaterial. Set of experiments with M-CN_x from another batch (batch II) of CN_x was repeated, and the same results were obtained, where M-CN_x showed not a negative effect on cell proliferation (Fig. 5).

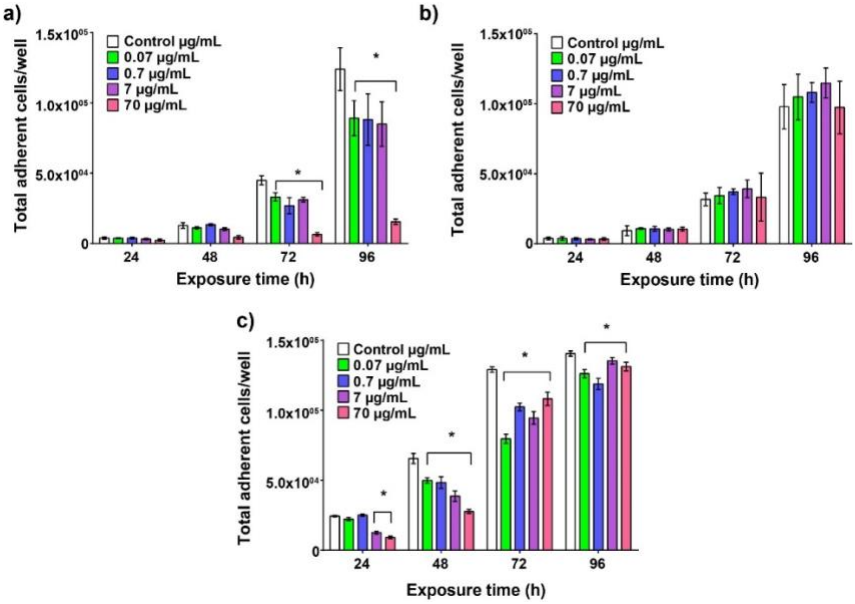

Fig. 4 Maximum cell growth of murine fibroblast exposed to different concentration of **a** S-CN_x, **b** M- CN_x, **c** L-CN_x. Data are presented as mean ± SD. n≥3

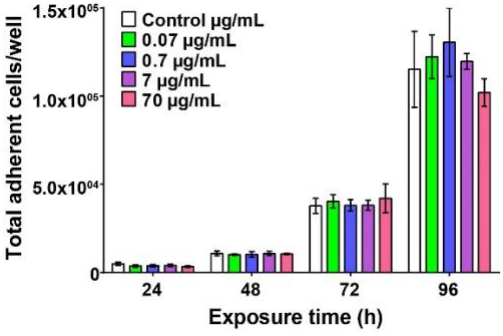

Fig. 5 Kinetic of growth of murine fibroblasts exposed to M-CN_x from batch II. Data are presented as mean ± SD, n≥3

The 50% inhibitory concentration (IC_{50}) of S-CN_x and L-CN_x was calculated at set time points (Electronic Supplementary Fig. 1a-b). At 48 h of exposure, the IC_{50} of both S-CN_x and L-CN_x were 24.03±7.02 µg/mL and 25.55±7.23 µg/mL, respectively. While cell viability sharply dropped at high concentration of S-CN_x, L-CN_x

demonstrated a gradual decrease in cell viability (Fig. 6a). Maximal cytotoxicity of S-CN_x was observed at 96 h of exposure with an IC_{50} of 3.03±1.35 µg/mL, while L-CN_x demonstrated its maximal toxic effect at 48 h (Fig. 6b). It's well known that pristine MWCNT shows more cytotoxicity than chemically modified MWCNT (Carrero-Sanchez et al. 2006; He et al. 2017; Li and Niu 2003; Zhao et al. 2011b; Zhou et al. 2017) and the cellular response to nanomaterials is also influenced by the cell type (Canapè et al. 2015; Sohaebuddin et al. 2010). Canapè et al. (2015) evaluated the effects of different carbon nanomaterials on several cell lines, where the same material shows both biocompatibility and cytotoxicity having different IC_{50} depending on the cell type. It was found that the IC_{50} values of S-CN_x and L-CN_x were similar to the ones reported in the literature (Canapè et al. 2015; Xiao et al. 2012; Zhou et al. 2017).

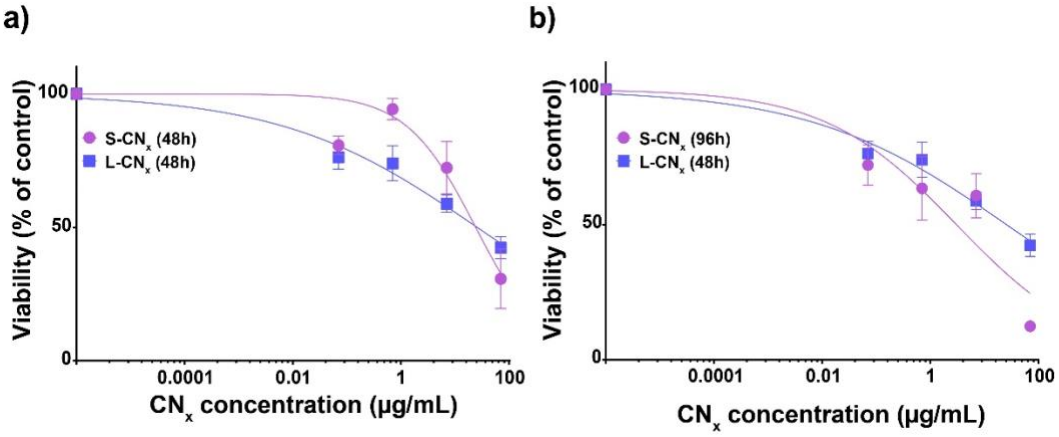

Fig. 6 a Comparative cell viability curve of NIH-3T3 fibroblast exposed to S-CN_x or L-CN_x at concentrations 0.07-70 µg/mL during 48 h. **b** Comparison between the maximum toxicity effect of S-CN_x and L-CN_x on murine cells found at different incubation times. Viability in treated samples was normalized with the untreated control, which was taken as 100%. Data are presented as mean ± SD. n≥3

Several studies have been done to evaluate the effects of CNTs on mammalian cells, showing that size and diameters of nanomaterial play a key role in the compatibility these nanomaterials (Fisher et al. 2012; Mihalchik et al. 2015; Sohaebuddin et al. 2010). As previous reported by other authors, the results obtained from murine fibroblasts exposed to CN_x suggested that the biocompatibility of CN_x depends on the size of the nanomaterial: However, the mechanisms are not entirely understood until now. One hypothesis is the type of nitrogen configuration on the CN_x. It has been reported that the type of nitrogen bond changes depending on the site of CN_x synthesis. At the beginning of the reactor, pyridinic and quaternary nitrogen have an essential contribution to get an order on the graphitic network. Despite that M-CN_x and L-CN_x are too close in the reactor (less than 6 cm of distance), the concentration of quaternary nitrogen and NO_x bonds is higher in M-CN_x compared with L-CN_x. In the case of pyrrolic-N and molecular nitrogen, the percentage of these bonds is higher in L-CN_x(Muñoz-Sandoval et al. 2018; Sanchez-Salas 2015). The difference in C≡N bonds content among L-CN_x, M-CN_x, and S-CN_x found in this work (Fig. 3) could also contribute to the explanation of why CN_x from the same batch showed both biocompatibility and cytotoxicity effects on mammalian fibroblast.

Effect of M-CN_x on trypsin-stressed fibroblasts

In vivo adherent cells are detached by endoproteases to make their functions such as cell motility, migration, cell division, or wound healing (McAnulty 2007). A previous report showed that trypsin-treated cells are more susceptible to CN_x, presenting a diminution on cell proliferation (Munguía-Lopez et al. 2015). To elucidate if M-CN_x are toxic for fibroblast enzymatically stressed, nanomaterials were incubated with cells immediately after the cell-liftoff with trypsin. Fig. 7 shows the trypsin-stressed fibroblasts kinetics in the presence of M-CN_x from two different batches of production. After 72 h of exposure to 7 µg/mL of M-CN_x, cell proliferation decreased significantly compared to control. Whereas increasing the concentration of M-CN_x to 70 µg/mL, after 48 h of exposure, cell proliferation was completely inhibited (Fig. 7a and b).

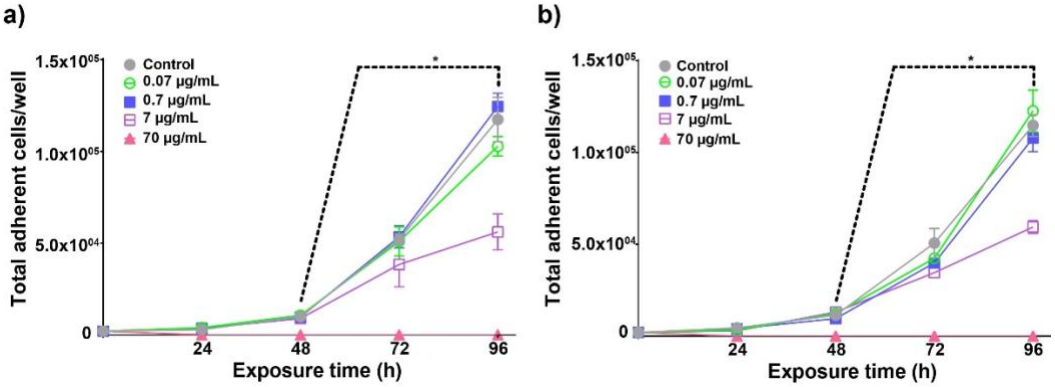

Fig. 7 Trypsin-stressed fibroblast cells exposed to different concentration of M-CN_x from **a** batch I or **b** batch II. Data are presented as mean ± SD.; n≥3

Morphology of the trypsin-stressed fibroblasts exposed to M-CN_x was analyzed by light microscopy. Fig. 8 shows a gallery of optical images from cells incubated with CN_x after 24 h. As noted, contrary to the images of control cultures (Fig. 8a and d), cells attached to carbon nanotubes instead of plate surface (Fig. 8b and c). At 96 h, cell agglomerations were observed on M-CN_x (Fig. 8e and f) and no cells attached to plate surface were found at the end of the culture. These results suggest that trypsin-stressed cells were susceptible to M-CN_x when they were exposed immediately to the nanomaterial after trypsinization, whereas the cells pre-incubated 24h before the treatment tolerated well the presence of CN_x.

As above mentioned, adherent cells secret endoproteases that allow them to detach from the surface to perform their biological functions (McAnulty 2007). This enzymatic digestion cut off proteins from the extracellular matrix (collagen, fibronectin) as well as transmembrane proteins such as integrins (Canavan et al. 2005). *In vitro*, the trypsin enzyme is used in routine cells culture protocols to detach cells from the plate; the enzymatic reaction is similar than occurs *in vivo*. In this context, it was found that trypsin-stressed cells preferred M-CN_x as surface instead of plate treated dishes suggesting high-cell affinity for nanomaterials and making them attractive for tissue regeneration. It has been reported that cells prefer CNTs as surfaces instead of standard culture plate surfaces for example glass, plastic, carbon paper (Hirata et al. 2012; Matsuoka et al. 2010; Ryoo et al. 2010; Zhao et al. 2011b). The trypsin-cell treatment creates small fragments of adhesion proteins that could interact directly with M-CN_x due

to their high affinity, blocking the cell adhesion to the surface plate and altering the extracellular matrix metabolism(Kaiser et al. 2013; McAnulty 2007).

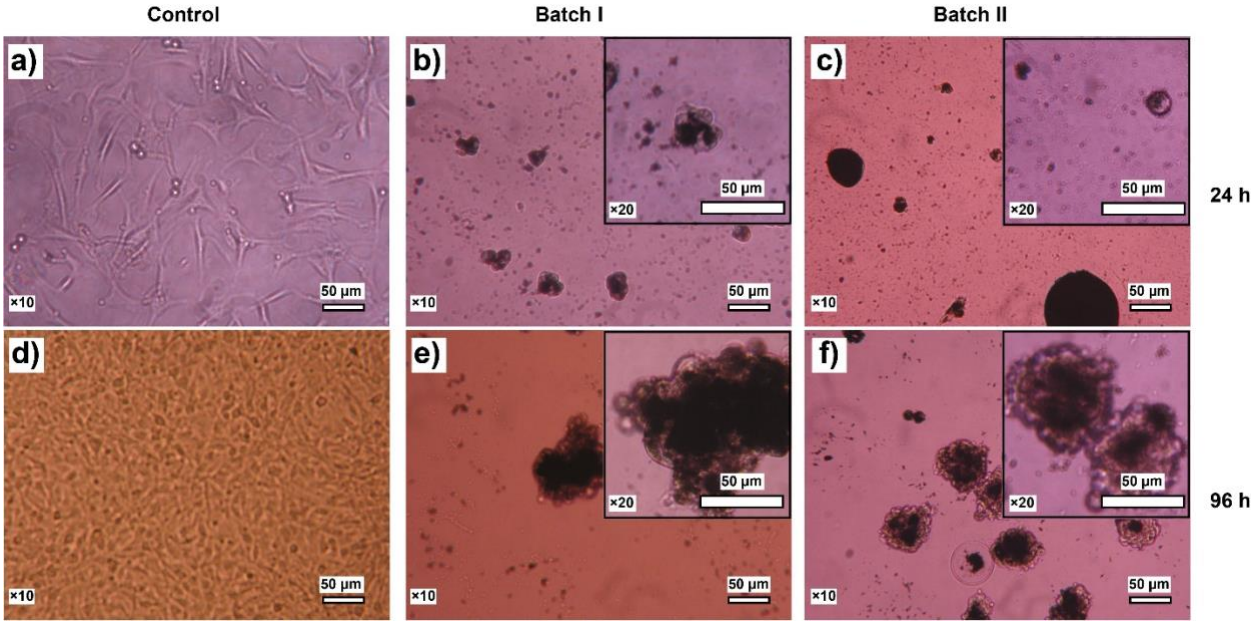

Fig. 8 Light microscopy images of stressed fibroblasts incubated with 70 µg/mL M-CN_x. **a, d** Control, cells with CN_x from **b, e** batch I or **c, f** batch II

Biocompatibility of CN_x on human hematopoietic stem cells

Since M-CN_x were the most biocompatible nanomaterial with murine fibroblasts when they were exposed after 24 h cell-liftoff, and the human umbilical cordon blood samples availability was limited, the biocompatibility tests were performed on hHSC cultures only with M-CN_x in the range of 0.07 to 70 µg/mL. Fig. 9 shows the expansion kinetic of hHSC with or without the nanomaterial for 120 h. As noted, the growth curves of cultures with CN_x were identical to the control cultures. Similar to murine fibroblasts cultures, M-CN_x from a different batch of production had no adverse effect on the expansion of hHSC (Fig. 9a and b). The TNF-α level was determined in control and 70 µg/mL of M-CN_x samples at the end of the kinetic, where control showed more production of TNF-α than samples with nanomaterials (Fig. 9c). These results suggest that M-CN_x were biocompatible with hHSC expansion. Bari et al. (2013) reported that carboxylic acid functionalized single-walled carbon nanotubes (f-SWCNT-COOH) has a protective role on hHSC cultures, where the exposure to these materials increase the viability of $CD45^+$ cells with a reduction in mitochondrial superoxides and caspase activity. Furthermore, the authors found that f-SWCNT-COOH reduce the portion of $CD45^-$ cells. Also, the authors reported that the surface functional group of SWCNT plays an important role in hHSC expansion.

Comparing the cellular response to f-SWCNT-O-NH_2, f-SWCNT-PEG, and f-SWCNT-COOH (amide, polyethylene-glycol, and carboxylic acid functionalized, respectively), all nanomaterials reduce the mitochondrial superoxides; however, f-SWCNT-COOH shows to be the best candidate for *ex vivo* expansion of hematopoietic

stem and progenitor cells, giving optimal viability support with the maximum reduction of mitochondrial superoxides (Bari et al. 2015).

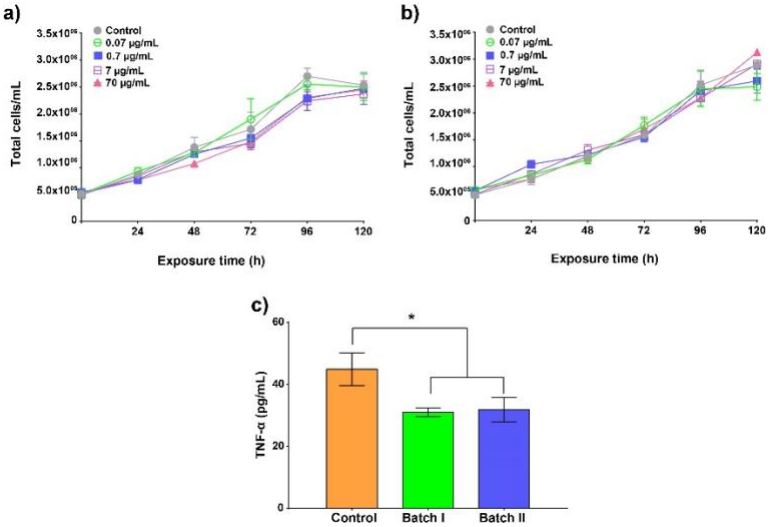

Fig 9 Expansion of hHSC incubated during 120 h with M-CN_x from **a** batch I or **b** batch II. **c** Determination of TNF-α level in cultures. Data are presented as mean ± SD. n≥3

Cellular uptake of CN_x on murine macrophages and human hematopoietic stem cells

Murine macrophages were exposed to 70 µg/mL of L-CN_x, M-CN_x or S-CN_x for cellular uptake experiments (Fig. 10). Based on optical imaging, macrophages embedded L-CN_x (Fig. 10b and f) and M-CNx (Fig. 10c and g), but not S-CN_x; instead, the nanomaterial formed agglomeration which attached to the surface of the macrophages forming nanomaterial-cell agglomeration complex (Fig. 10d and h). The cell concentration after 24 h in S-CN_x culture was lower that M-CN_x and L-CN_x cultures ($6.4\pm1.3x10^3$ cell/well *vs.* 3.8 ± 0.6 $x10^4$ and 3.7 ± 0.8 $x10^4$ cells/well, respectively). At 48 h, similar results on cell concentration were found, where S-CN_x cultures showed the lowest cell quantity per well. As previously mentioned, S-CN_x-macrophages agglomeration complexes were found attached to the surface plate culture and based on naked-eye assessment, the majority of S-CN_x were not embedded by cells; therefore, S-CN_x culture were discarded from quantification analysis.

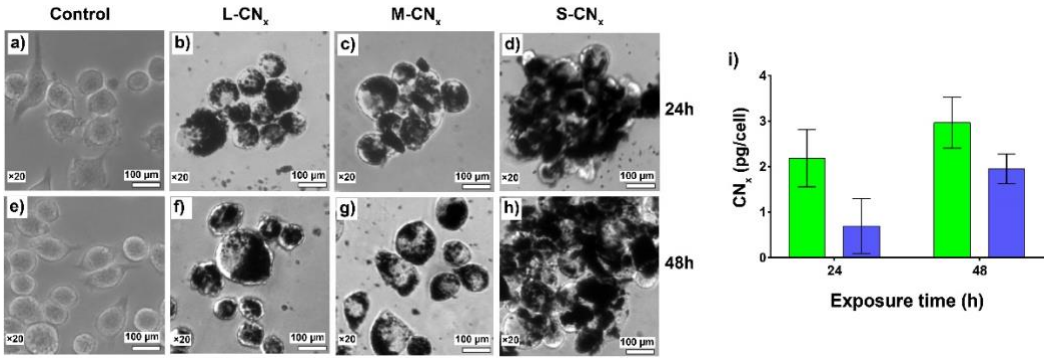

Fig. 10 Optical images of CN_x cellular uptake by macrophages J774a.1. **a, e** control; **b, f** L-CN_x; **c, g** M-CN_x; **d, h** S-CN_x cultures. **i** Concentration of CN_x uptake by cells. Data are presented as mean ± SD.; n≥3

Different strategies have been used for nanomaterial cellular uptake quantification such as radiolabeling (Zhang et al. 2012b; Zhang et al. 2010; Zhang et al. 2011a), gel electrophoresis (Cui et al. 2017) and UV-Vis-NIR spectroscopy (Zhang et al. 2018). The latter technique has been demonstrated to be a good technique to quantify cellular uptake of nanomaterials in the NIR region with minimum interference of biological molecules (Weissleder 2001; Zhang et al. 2012a). For nanotubes quantification, M-CN_x and L-CN_x cultures were washed with PBS and nanomaterials were extracted from cells by ultrasonic lysis and centrifuge cycles. The CN_x concentrations uptake by cells were estimated based on the cell number and the corresponding calibration curves (Electronic Supplementary Fig. 2a-b). Macrophages uptake 2.18±0.62 pg/cell and 0.69±0.60 pg/cell of M-CN_x and L-CN_x, respectively after 24 h of exposure; a slight increment in cellular uptake at 48 h was detected in both M-CN_x and L-CN_x cultures but with no significant difference was observed (2.96±0.55 pg/cell and 1.94±0.32 pg/cell respectively) (Fig. 10i).

Cellular uptake efficiency is associated with nanomaterial physicochemical properties as well as cell types. Zhang et al. (2012b) studied the cellular uptake and cytotoxicity of carbon nanomaterials (CNM) on HeLa cells. The CNM employed for their research were MWCNTs, graphene oxide (GO) and nanodiamonds (ND). According to their results, the authors found that CNM are readily internalized by HeLa cells in nonspecific cellular uptake with significant differences in internalization ratios, where cells internalized higher concentration of ND, followed by MWCNT and GO. Furthermore, the CNM show a dose- and time-dependent cytotoxicity but their toxicity was not associated with their cell uptake ratios since ND exhibit the highest cellular uptake with least cytotoxicity.

Regarding the size-dependent uptake, Zhang et al. (2018) employed eight commercially available CNTs with different sizes to study the nanomaterial internalization by macrophages RAW264.7. Among the CNTs used, two of them were SWCNTs and six MWCNTs, all of which have different surface areas, diameters, and Raman intensity ratios (G/D). Based on UV-Vis-NIR measurements, the largest CNTs (≈390 nm) show the highest cellular uptake (≈75 pg/cell), and the smallest CNTs show the lowest uptake (≈1.5pg/cells). The CNTs with similar sizes show similar cellular uptake (≈2-3 pg/cell). According to the authors, the cellular uptake of CNTs by macrophages depends on their sizes, regardless of type or manufacturer; furthermore, the internalization of CNTs increase linearly with the dynamic size and the toxicity increase along with uptake. In this work, despite the difference in physicochemical properties and sizes of M-CN_x and L-CN_x, the M-CN_x cellular uptake was slightly higher that L-CN_x at 24 h of exposure, but at 48 h the cellular uptake was similar, suggesting that macrophages J774a.1 can internalize both kinds of CN_x in a time-dependent manner.

Following the CN_x cellular uptake studies, Fig. 11 shows the light microscopy of hHSC after incubation during 120 h with M-CN_x at 70 µg/mL. Apparently, some cells phagocyted the nanomaterial (Fig. 11a and b). To confirm if the nanomaterials were located inside of the cells, several washes were carried out to eliminate M-CN_x from the culture medium or outside of the cells. After washing process, cells kept the nanomaterials inside suggesting that M-CN_x were phagocyted (Fig. 11c and d).

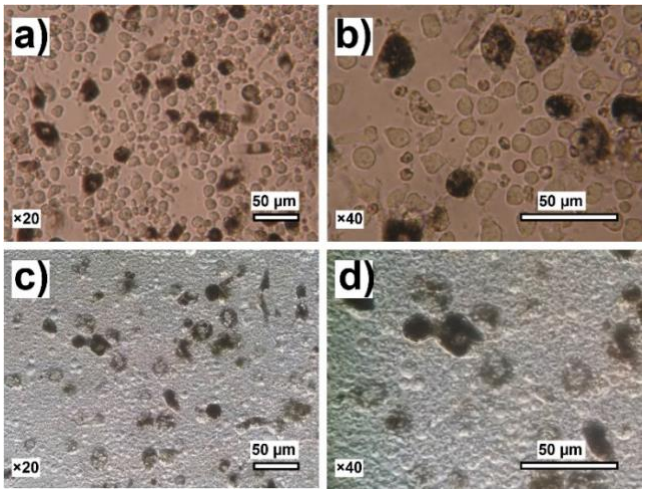

Fig. 11 Cellular uptake images of hHSC after incubation during 120 h with M-CN_x at 70 µg/mL. **a, b** images were taken in presence of culture medium and **c, d** after PBS washing

M-CN_x were recovered from cells by cell lysis and Fig. 12 shows the SEM images of M-CN_x as well as their EDX spectrum. Nanomaterials sonicated in ethanol were found as well defined and dispersed M-CN_x (Fig. 12a) with the presence of carbon, oxygen and sulfur elements, corresponding to SO_4^- groups generate by purification process (Fig. 12d). M-CN_x dispersed in basal-IMDM showed well dispersion but nanomaterials were covered by proteins form FBS, creating a thick layer making difficult to see individual M-CN_x (Fig. 12b), the EDX analysis exhibited the presence of some of the elements present in the culture medium (Fig. 12e). The M-CN_x extracted from cells were observed as individual sharply-nanotubes as well as CN_x-bundles forming agglomerations with biological material; these agglomerations could be due to the interaction between CN_x and intracellular biomolecules (Fig. 12c, yellow arrows). The EDX spectra showed the elements present in the sample (Fig. 12f). Due to M-CN_x dispersed in basal-IMDM and M-CN_x extracted from cells had different morphology as well as differences in their EDX spectra, it can be inferred that M-CN_x were phagocyted by the hHSC. Cells uptake nanomaterials by energy-dependent and -independent mechanisms depend on the material properties (Pulskamp et al. 2007; Zhao et al. 2011a). It has been reported that the internalization of CNTs by cells caused the non-specific interaction (hydrogen bonding, van der Waals, electrostatic, hydrophobic, etc.) with intracellular macromolecules such as protein, DNA, RNA, carbohydrates or lipids (Blazer-Yost et al. 2011; Li et al. 2014; Meng et al. 2005). Based on SEM and EDX spectra of M-CN_x, the morphological and chemical composition showed differences, suggesting that CN_x phagocyted by hHSC adsorbed biological macromolecules.

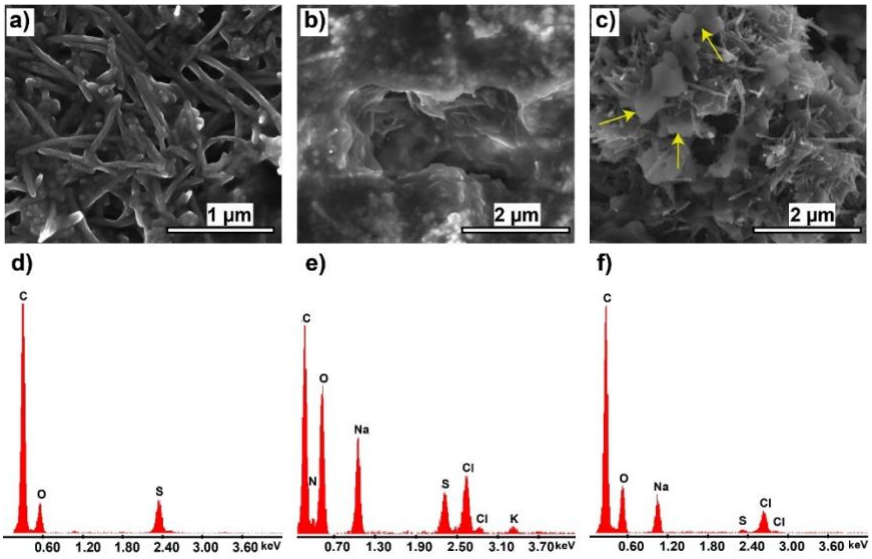

Fig. 12 SEM imaging and EDX analysis of M-CN_x. **a** SEM micrograph of M-CN_x dispersed in ethanol, **b** basal-IMDM and **c** extracted from cells. **d-f** Respective EDX spectra of the samples

5. Conclusions

In this work, it has been demonstrated that CVD synthesis produces different nanomaterials morphologies, which generate differences in the cellular response. The three CN_x used here show differences in sizes and chemical composition, where S-CNx ranging 0.07 to 7 µg/mL, and L-CN_x 0.07 to 70 µg/mL are slightly cytotoxic for the murine fibroblasts, and 70 µg/mL S-CN_x are cytotoxic for the murine cells showing the lowest IC_{50}. Whereas M-CN_x in the range of 0.07 to 70 µg/mL are biocompatible with mammalian cells such as NIH-3T3 murine fibroblast and human hematopoietic stem cells, and they can phagocyte them. In terms of cellular uptake, murine macrophages can phagocytose both M-CN_x and L-CN_x at a similar rate. However, S-CN_x formed nanomaterial-cell agglomerates complexes are not phagocytosed by these cells. Along with the nanomaterial sizes, the nitrogen configuration and content in the CN_x play an important role for determining the biocompatibility of the nanomaterials. Although further studies should be performed to fully understand the biological response to these CN_x and improvements should be made in CN_x synthesis and recovery; the M-CN_x could be a great candidate for biomedical applications.

Funding: The authors thank The Marcos Moshinsky Foundation, CONACYT-Mexico CB-2013-220744 for partial funding and CONACYT for the scholarship 250279. Also, the authors thank L. Aldana and Abdullah Chaudhary for the English review and V. Balderas for his technical assistance.

Conflicts of Interest: The authors declare that they have no conflict of interest.

References

Andrade-Zaldívar H, Kalixto-Sánchez MA, de la Rosa APB, De León-Rodríguez A (2011) Expansion of Human Hematopoietic Cells from Umbilical Cord Blood Using Roller Bottles in CO2 and CO2-Free Atmosphere Stem Cells and Development 20:593-598 doi:10.1089/scd.2010.0236

Bari S et al. (2015) Mitochondrial superoxide reduction and cytokine secretion skewing by carbon nanotube scaffolds enhance ex vivo expansion of human cord blood hematopoietic progenitors Nanomedicine : nanotechnology, biology, and medicine 11:1643-1656 doi:10.1016/j.nano.2015.06.005

Bari S et al. (2013) Protective role of functionalized single walled carbon nanotubes enhance ex vivo expansion of hematopoietic stem and progenitor cells in human umbilical cord blood Nanomedicine : nanotechnology, biology, and medicine 9:1304-1316 doi:10.1016/j.nano.2013.05.009

Bazargan A, McKay G (2012) A review – Synthesis of carbon nanotubes from plastic wastes Chemical Engineering Journal 195-196:377-391 doi:10.1016/j.cej.2012.03.077

Blazer-Yost BL et al. (2011) Effect of carbon nanoparticles on renal epithelial cell structure, barrier function, and protein expression Nanotoxicology 5:354-371 doi:10.3109/17435390.2010.514076

Canapè C, Foillard S, Bonafè R, Maiocchi A, Doris E (2015) Comparative assessment of the in vitro toxicity of some functionalized carbon nanotubes and fullerenes RSC Advances 5:68446-68453 doi:10.1039/c5ra11489f

Canavan HE, Cheng X, Graham DJ, Ratner BD, Castner DG (2005) Cell sheet detachment affects the extracellular matrix: A surface science study comparing thermal liftoff, enzymatic, and mechanical methods Journal of Biomedical Materials Research Part A 75A:1-13 doi:10.1002/jbm.a.30297

Carrero-Sanchez JC, Elias AL, Mancilla R, Arrellin G, Terrones H, Laclette JP, Terrones M (2006) Biocompatibility and toxicological studies of carbon nanotubes doped with nitrogen Nano Lett 6:1609-1616 doi:10.1021/nl060548p

Cui HF, Vashist SK, Al-Rubeaan K, Luong JH, Sheu FS (2010) Interfacing carbon nanotubes with living mammalian cells and cytotoxicity issues Chem Res Toxicol 23:1131-1147 doi:10.1021/tx100050h

Cui X, Wan B, Yang Y, Ren X, Guo LH (2017) Length effects on the dynamic process of cellular uptake and exocytosis of single-walled carbon nanotubes in murine macrophage cells Sci Rep 7:1518 doi:10.1038/s41598-017-01746-9

De Volder MF, Tawfick SH, Baughman RH, Hart AJ (2013) Carbon nanotubes: present and future commercial applications Science 339:535-539 doi:10.1126/science.1222453

Escobar Barrios VA, Rangel Méndez JR, Pérez Aguilar NV, Andrade Espinosa G, Dávila Rodríguez JL (2012) FTIR - An Essential Characterization Technique for Polymeric Materials. In: Theophanides T (ed) Infrared Spectroscopy. IntechOpen. doi:10.5772/36044

Ferreira L, Karp JM, Nobre L, Langer R (2008) New Opportunities: The Use of Nanotechnologies to Manipulate and Track Stem Cells Cell Stem Cell 3:136-146 doi:10.1016/j.stem.2008.07.020

Fisher C, E. Rider A, Jun Han Z, Kumar S, Levchenko I, Ostrikov K (2012) Applications and Nanotoxicity of Carbon Nanotubes and Graphene in Biomedicine Journal of Nanomaterials 2012:1-19 doi:10.1155/2012/315185

He S et al. (2017) Biocompatible carbon nanotube fibers for implantable supercapacitors Carbon 122:162-167 doi:10.1016/j.carbon.2017.06.053

Hirata E, Akasaka T, Uo M, Takita H, Watari F, Yokoyama A (2012) Carbon nanotube-coating accelerated cell adhesion and proliferation on poly (L-lactide) Applied Surface Science 262:24-27 doi:10.1016/j.apsusc.2012.01.012

Huang L, Liu M, Huang H, Wen Y, Zhang X, Wei Y (2018) Recent Advances and Progress on Melanin-like Materials and Their Biomedical Applications Biomacromolecules 19:1858-1868 doi:10.1021/acs.biomac.8b00437

Jiang K et al. (2003) Selective Attachment of Gold Nanoparticles to Nitrogen-Doped Carbon Nanotubes Nano Letters 3:275-277 doi:10.1021/nl025914t

Jourdain V, Bichara C (2013) Current understanding of the growth of carbon nanotubes in catalytic chemical vapour deposition Carbon 58:2-39 doi:10.1016/j.carbon.2013.02.046

Kaiser JP, Buerki-Thurnherr T, Wick P (2013) Influence of single walled carbon nanotubes at subtoxical concentrations on cell adhesion and other cell parameters of human epithelial cells Journal of King Saud University - Science 25:15-27 doi:10.1016/j.jksus.2012.06.003
Kamalakaran R et al. (2000) Synthesis of thick and crystalline nanotube arrays by spray pyrolysis Applied Physics Letters 77:3385-3387
Kim AD, Stachura DL, Traver D (2014) Cell signaling pathways involved in hematopoietic stem cell specification Exp Cell Res 329:227-233 doi:10.1016/j.yexcr.2014.10.011
Krenning G, Zeisberg EM, Kalluri R (2010) The origin of fibroblasts and mechanism of cardiac fibrosis Journal of Cellular Physiology 225:631-637 doi:10.1002/jcp.22322
Kunzmann A, Andersson B, Thurnherr T, Krug H, Scheynius A, Fadeel B (2011) Toxicology of engineered nanomaterials: Focus on biocompatibility, biodistribution and biodegradation Biochimica et Biophysica Acta (BBA) - General Subjects 1810:361-373 doi:10.1016/j.bbagen.2010.04.007
Lanone S, Andujar P, Kermanizadeh A, Boczkowski J (2013) Determinants of carbon nanotube toxicity Adv Drug Deliv Rev doi:10.1016/j.addr.2013.07.019
Li DJ, Niu LF (2003) Influence of N atomic percentages on cell attachment for CNx coatings Bull Mater Sci 26:371-375 doi:10.1007/BF02711178
Li L, Lin R, He H, Sun M, Jiang L, Gao M (2014) Interaction of amidated single-walled carbon nanotubes with protein by multiple spectroscopic methods Journal of Luminescence 145:125-131 doi:10.1016/j.jlumin.2013.07.008
Liao L, Pan C (2011) Enhanced Electrochemical Capacitance of Nitrogen-Doped Carbon Nanotubes Synthesized from Amine Flames Soft Nanoscience Letters 01:16-23 doi:10.4236/snl.2011.11004
Liu M et al. (2015) Self-polymerization of dopamine and polyethyleneimine: novel fluorescent organic nanoprobes for biological imaging applications Journal of Materials Chemistry B 3:3476-3482 doi:10.1039/c4tb02067g
Liu M, Zeng G, Wang K, Wan Q, Tao L, Zhang X, Wei Y (2016a) Recent developments in polydopamine: an emerging soft matter for surface modification and biomedical applications Nanoscale 8:16819-16840 doi:10.1039/c5nr09078d
Liu Y, Zhao Y, Sun B, Chen C (2013) Understanding the Toxicity of Carbon Nanotubes Acc Chem Res 46:702-713 doi:doi.org/10.1021/ar300028m
Liu Z et al. (2014) Carboxylation of multiwalled carbon nanotube enhanced its biocompatibility with L02 cells through decreased activation of mitochondrial apoptotic pathway Journal of biomedical materials research Part A 102:665-673 doi:10.1002/jbm.a.34729
Liu Z, Liu Y, Peng D (2016b) Hydroxylation of multi-walled carbon nanotubes: Enhanced biocompatibility through reduction of oxidative stress initiated cell membrane damage, cell cycle arrestment and extrinsic apoptotic pathway Environmental toxicology and pharmacology 47:124-130 doi:10.1016/j.etap.2016.09.013
Matsuoka M, Akasaka T, Totsuka Y, Watari F (2010) Strong adhesion of Saos-2 cells to multi-walled carbon nanotubes Materials Science and Engineering: B 173:182-186 doi:10.1016/j.mseb.2009.12.044
McAnulty RJ (2007) Fibroblasts and myofibroblasts: Their source, function and role in disease The International Journal of Biochemistry & Cell Biology 39:666-671 doi:10.1016/j.biocel.2006.11.005
Meng J, Song L, Xu H, Kong H, Wang C, Guo X, Xie S (2005) Effects of single-walled carbon nanotubes on the functions of plasma proteins and potentials in vascular prostheses Nanomedicine : nanotechnology, biology, and medicine 1:136-142 doi:10.1016/j.nano.2005.03.003
Meysami SS, Dillon F, Koós AA, Aslam Z, Grobert N (2013a) Aerosol-assisted chemical vapour deposition synthesis of multi-wall carbon nanotubes: I. Mapping the reactor Carbon 58:151-158 doi:10.1016/j.carbon.2013.02.044

Meysami SS, Koós AA, Dillon F, Grobert N (2013b) Aerosol-assisted chemical vapour deposition synthesis of multi-wall carbon nanotubes: II. An analytical study Carbon 58:159-169 doi:10.1016/j.carbon.2013.02.041
Mihalchik AL et al. (2015) Effects of nitrogen-doped multi-walled carbon nanotubes compared to pristine multi-walled carbon nanotubes on human small airway epithelial cells Toxicology doi:10.1016/j.tox.2015.03.008
Mubarak NM, Abdullah EC, Jayakumar NS, Sahu JN (2014) An overview on methods for the production of carbon nanotubes Journal of Industrial and Engineering Chemistry 20:1186-1197 doi:doi.org/10.1016/j.jiec.2013.09.001
Mundra RV, Wu X, Sauer J, Dordick JS, Kane RS (2014) Nanotubes in biological applications Current opinion in biotechnology 28:25-32 doi:10.1016/j.copbio.2013.10.012
Munguía-Lopez JG, Muñoz-Sandoval E, Ortiz-Medina J, Rodriguez-Macias FJ, De Leon-Rodriguez A (2015) Effects of Nitrogen-Doped Multiwall Carbon Nanotubes on Murine Fibroblasts Journal of Nanomaterials 2015:1-7 doi:10.1155/2015/801606
Muñoz-Sandoval E, Fajardo-Díaz JL, Sánchez-Salas R, Cortés-López AJ, López-Urías F (2018) Two Sprayer CVD Synthesis of Nitrogen-doped Carbon Sponge-type Nanomaterials Scientific Reports 8:2983 doi:10.1038/s41598-018-20079-9
Nxumalo EN, Nyamori VO, Coville NJ (2008) CVD synthesis of nitrogen doped carbon nanotubes using ferrocene/aniline mixtures Journal of Organometallic Chemistry 693:2942-2948 doi:10.1016/j.jorganchem.2008.06.015
Pulskamp K, Diabate S, Krug HF (2007) Carbon nanotubes show no sign of acute toxicity but induce intracellular reactive oxygen species in dependence on contaminants Toxicol Lett 168:58-74 doi:10.1016/j.toxlet.2006.11.001
Ryabenko AG, Dorofeeva TV, Zvereva GI (2004) UV–VIS–NIR spectroscopy study of sensitivity of single-wall carbon nanotubes to chemical processing and Van-der-Waals SWNT/SWNT interaction. Verification of the SWNT content measurements by absorption spectroscopy Carbon 42:1523-1535 doi:doi.org/10.1016/j.carbon.2004.02.005
Ryoo SR, Kim YK, Kim MH, Min DH (2010) Behaviors of NIH-3T3 fibroblasts on graphene/carbon nanotubes: proliferation, focal adhesion, and gene transfection studies ACS Nano 4:6587-6598 doi:10.1021/nn1018279
Sabuncu AC, Kalluri BS, Qian S, Stacey MW, Beskok A (2010) Dispersion state and toxicity of mwCNTs in cell culture medium with different T80 concentrations Colloids and Surfaces B: Biointerfaces 78:36-43 doi:10.1016/j.colsurfb.2010.02.005
Sanchez-Salas R (2015) Sintesis de nanotubos de carbono dopados con nitrogeno: un estudio sistemático. Instituto Potosino de Investigación Científica y Tecnológica, A.C (IPICyT)
Shah KA, Tali BA (2016) Synthesis of carbon nanotubes by catalytic chemical vapour deposition: A review on carbon sources, catalysts and substrates Materials Science in Semiconductor Processing 41:67-82 doi:10.1016/j.mssp.2015.08.013
Shi Y et al. (2017) Biomimetic PEGylation of carbon nanotubes through surface-initiated RAFT polymerization Mater Sci Eng C Mater Biol Appl 80:404-410 doi:10.1016/j.msec.2017.06.009
Sohaebuddin SK, Thevenot PT, Baker D, Eaton JW, Tang L (2010) Nanomaterial cytotoxicity is composition, size, and cell type dependent Particle and Fibre Toxicology 7:22 doi:10.1186/1743-8977-7-22
Tucureanu V, Matei A, Avram AM (2016) FTIR Spectroscopy for Carbon Family Study Crit Rev Anal Chem 46:502-520 doi:10.1080/10408347.2016.1157013
Wai Feng Lim , Tomoko Inoue-Yokoo , Keai Sinn Tan , Lai MI, Sugiyama D (2013) Hematopoietic cell differentiation from embryonic and induced pluripotent stem cell Stem Cell Research & Therapy 4:71
Weissleder R (2001) A clearer vision for in vivo imaging Nature Biotechnology 19:316-317 doi:10.1038/86684

Wu X, Tao Y, Lu Y, Dong L, Hu Z (2006) High-pressure pyrolysis of melamine route to nitrogen-doped conical hollow and bamboo-like carbon nanotubes Diamond and Related Materials 15:164-170 doi:10.1016/j.diamond.2005.09.018
Xiao H et al. (2012) Photodynamic effects of chlorin e6 attached to single wall carbon nanotubes through noncovalent interactions Carbon 50:1681-1689 doi:10.1016/j.carbon.2011.12.013
Zhang M et al. (2018) Size-dependent cell uptake of carbon nanotubes by macrophages: A comparative and quantitative study Carbon 127:93-101 doi:10.1016/j.carbon.2017.10.085
Zhang M, Zhou X, Iijima S, Yudasaka M (2012a) Small-sized carbon nanohorns enabling cellular uptake control Small 8:2524-2531 doi:10.1002/smll.201102595
Zhang X, Hu W, Li J, Tao L, Wei Y (2012b) A comparative study of cellular uptake and cytotoxicity of multi-walled carbon nanotubes, graphene oxide, and nanodiamond Toxicology Research 1 doi:10.1039/c2tx20006f
Zhang X, Huang Q, Deng F, Huang H, Wan Q, Liu M, Wei Y (2017) Mussel-inspired fabrication of functional materials and their environmental applications: Progress and prospects Applied Materials Today 7:222-238 doi:10.1016/j.apmt.2017.04.001
Zhang X et al. (2015) Interaction of tannic acid with carbon nanotubes: enhancement of dispersibility and biocompatibility Toxicology Research 4:160-168 doi:10.1039/c4tx00066h
Zhang X et al. (2012c) Biocompatible polydopamine fluorescent organic nanoparticles: facile preparation and cell imaging Nanoscale 4:5581-5584 doi:10.1039/c2nr31281f
Zhang X et al. (2010) Biodistribution and toxicity of nanodiamonds in mice after intratracheal instillation Toxicol Lett 198:237-243 doi:10.1016/j.toxlet.2010.07.001
Zhang X et al. (2011a) Distribution and biocompatibility studies of graphene oxide in mice after intravenous administration Carbon 49:986-995 doi:10.1016/j.carbon.2010.11.005
Zhang X, Zhu Y, Li J, Zhu Z, Li J, Li W, Huang Q (2011b) Tuning the cellular uptake and cytotoxicity of carbon nanotubes by surface hydroxylation Journal of Nanoparticle Research 13:6941-6952 doi:10.1007/s11051-011-0603-9
Zhao F, Zhao Y, Liu Y, Chang X, Chen C, Zhao Y (2011a) Cellular uptake, intracellular trafficking, and cytotoxicity of nanomaterials Small 7:1322-1337 doi:10.1002/smll.201100001
Zhao ML, Li DJ, Yuan L, Yue YC, Liu H, Sun X (2011b) Differences in cytocompatibility and hemocompatibility between carbon nanotubes and nitrogen-doped carbon nanotubes Carbon 49:3125-3133 doi:10.1016/j.carbon.2011.03.037
Zhao X, Liu R (2012) Recent progress and perspectives on the toxicity of carbon nanotubes at organism, organ, cell, and biomacromolecule levels Environment International 40:244-255 doi:10.1016/j.envint.2011.12.003
Zhou L, Forman HJ, Ge Y, Lunec J (2017) Multi-walled carbon nanotubes: A cytotoxicity study in relation to functionalization, dose and dispersion Toxicol In Vitro 42:292-298 doi:10.1016/j.tiv.2017.04.027
Zhu Y, Li W, Li Q, Li Y, Li Y, Zhang X, Huang Q (2009) Effects of serum proteins on intracellular uptake and cytotoxicity of carbon nanoparticles Carbon 47:1351-1358 doi:10.1016/j.carbon.2009.01.026